May 2022

Development of Stabilized Zero Valent Iron Nanoparticles for Environmental Remediation Using Fractioned Humic Acid

Ruth Margaret Ntabala
University of Wisconsin-Milwaukee

DEVELOPMENT OF STABILIZED ZERO VALENT IRON NANOPARTICLES FOR ENVIRONMENTAL REMEDIATION USING FRACTIONED HUMIC ACID

by

Ruth Margaret Ntabala

A Thesis Submitted in

Partial Fulfillment of the

Requirements for the Degree of

Master of Science

in Geosciences

at The University of Wisconsin-Milwaukee

May 2022

ABSTRACT

DEVELOPMENT OF IMPROVED ZERO VALENT IRON NANOPARTICLES FOR ENVIRONMENTAL REMEDIAION USING FRACTIONED HUMIC SUBSTANCES

by

Ruth Margaret Ntabala

The University of Wisconsin – Milwaukee, 2022
Under the Supervision of Professor Shangping Xu, PhD

Nanosized zero valent iron (NZVI) is a new technology used for the treatment of contaminated water, soil, and sediment. Remediation by NZVI of subsurface contaminants is conducted by the injection of NZVI into the contaminated area, however, there are challenges when applying NZVI in the subsurface. These challenges include aggregation, low mobility, and environmental and ecological risks. Research has been conducted to modify the surface properties of NZVI using different coatings to combat these problems. However, these coatings usually involve synthesized chemicals and have only dealt with one or two of these challenges. There is a need for the development of coated NZVI that is low-cost, stable, environmentally compatible, reactive and has controlled mobility. The focus of this research is to use size-fractioned natural humic acid to coat the surface of synthesized NZVI and to test their effects on the NZVI stability under systematically design chemistry conditions. The results from this study showed that humic acid coating, particularly small size fractions of humic acid, could significantly increase the stability of NZVI under extremely high NaCl concentrations and moderate $CaCl_2$ concentrations. The extended Derjaguin, Landau, Verwey and Overbeek (XDLVO) theory was applied to correlate the particle-particle energy interactions to NZVI stability.

TABLE OF CONTENTS

LIST OF FIGURES

LIST OF TABLES

ACKNOWLEDGMENTS

Firstly, I wish to express my sincere appreciation to my advisor Dr. Shangping Xu for his counsel and support during my research. He provided me with valuable resources and continued to be supportive and understanding in my unusual circumstance of having a child during the second semester of my graduate program. I would like to thank Dr. Haiyan Yang for her guidance and help with my lab work. Her contributions were fundamental for the completion of my research. I would like to express my gratitude to Dr. Yin Wang for his support and guidance. I would like to thank Marianna Orlova from the biology department for training me on the ultracentrifuge and Pat Anderson from the School of Freshwater Sciences for his help with AA and TOC measurements. I would like to thank Hui Lin and Dr. Laodong Guo for their help with the humic acid characterization. I would like to acknowledge Dr. Marcia Silva for allowing me the use of her Zetasizer equipment and Dr. Steve Hardcastle for giving me access to his XRD equipment. I would also like to thank Dr. Timothy Grundl for his feedback on my research.

Lastly, I would like to thank my family and my husband for all their support.

1. Introduction

Nanosized zero valent iron (NZVI) particles were effective for the removal and/or degradation of a wide range of pollutants such as chlorinated organic solvents, chlorinated pesticides, organophosphates, polychlorinated biphenyls (PCBs), azo dyes, antibiotics, heavy metals and metalloids, nitrate and perchlorate (Crane and Scott 2012, O'Carroll, Sleep et al. 2013, Fu, Dionysiou et al. 2014, Guan, Sun et al. 2015, Lefevre, Bossa et al. 2016, Stefaniuk, Oleszczuk et al. 2016, Zhao, Liu et al. 2016). The mechanisms through which NZVI removes contaminants include chemical reduction and surface adsorption/precipitation. The application of NZVI for the remediation of subsurface contaminants usually involves the injection of NZVI, which will subsequently spread with the groundwater flow to target the pollutant plume. Currently, a major challenges for the subsurface application of NZVI include the aggregation of NZVI particles in aqueous solution (Phenrat, Saleh et al. 2007, Crane and Scott 2012, Dong, Zhao et al. 2016) as well as the low mobility of NZVI within the subsurface system (Kanel, Goswami et al. 2008, Crane and Scott 2012, Su, Puls et al. 2013, Mystrioti, Papassiopi et al. 2015). Phenrat et al. (2007), for instance, observed that the size of NZVI particles could grow from 20 nm to > 1 μm within 10 minutes. These aggregates can assemble themselves into clusters with sizes ~20-70 μm in 30 minutes. Such aggregation process can significantly lower the surface area, activity and mobility of NZVI within the subsurface system and subsequently limit their effectiveness for *in-situ* environmental remediation. Such particle aggregation could facilitate the attachment/straining of the NZVI to/by the soil and sediments and lead to very limited NZVI mobility. Su et al. (2013) showed that the travel distance of NZVI from the injection site was 0.89-2.1m, depending on the injection technique that was employed.

Experiments performed by Kanel et al. (2008) suggested that there was virtually no transport of NZVI within a simulated groundwater system.

Attempts were made to modify the surface properties of NZVI to improve their stability (Kanel, Goswami et al. 2008, Grieger, Fjordbøge et al. 2010, Crane and Scott 2012, Raychoudhury, Tufenkji et al. 2012, O'Carroll, Sleep et al. 2013, Esfahani, Firouzi et al. 2014, Fu, Dionysiou et al. 2014, Zhou, Thanh et al. 2014, Guan, Sun et al. 2015, Mystrioti, Papassiopi et al. 2015, Chekli, Brunetti et al. 2016, Dong, Xie et al. 2016, Dong, Zhao et al. 2016, Lefevre, Bossa et al. 2016, Li, Rajasekar et al. 2016, Stefaniuk, Oleszczuk et al. 2016, Zhao, Liu et al. 2016, Dong, Zhao et al. 2017). Surfactants and polyelectrolyte coatings such as butyl methacrylate, carboxymethyl cellulose, guar gum, polyacrylic acid, polyaspartate and so on have been tested with varying success. Saleh et al. (2006) used an anionic surfactant, sodium dodecylbenzene-sulfonic acid (SDBS) to coat a commercial NZVI and reported that SDBS significantly increased the stability of the NZVI through enhancing surface negative charges and thus electrostatic repulsion. Additionally, SDBS also increased the mobility of NZVI as the smaller sizes of the stable NZVI was less susceptible to physical straining (caused by particle aggregation) and clogging. He and Zhao (2007) produced stable NZVI particles of 18.6 nm in size using carboxymethyl cellulose (CMC) that has a molecular weight of 90,000 Dalton. The stabilization of the NZVI was attributed to the negative charges that originate from CMC molecules. The CMC-stabilized NZVI were shown to display significantly higher mobility within saturated sand and sandy soil (He, Zhang et al. 2009, Raychoudhury, Tufenkji et al. 2012, Li, Rajasekar et al. 2016).

Despite the advances in the modification of NZVI for environmental remediation purposes, key challenges remain for the successful use of NZVI for environmental remediation

applications. Particularly, there is a need for the development of low-cost, stable and environmentally compatible NZVI with enhanced stability. The use of natural organic matter (NOM) as a coating on NZVI has been shown to influence the fate and reactivity of NZVI (Li, et al., 2018). It was found that NOM may inhibit NZVI reactivity with target pollutants, lowering the removal efficiency (Chen et al., 2011). However, it was also found that in the degradation of compounds by NZVI, NOM may act as an electron-transfer mediator. Humic acid has been found to have both inhibitory (Giasuddin et al., 2007; Niu et al., 2011) and stimulatory effects (Feng et al., 2008) on the reactivity of NZVI. Molecular weight of a particle has been found to influence the absorbance onto NZVI (Li, et al., 2018). The research that has been conducted on the effects of HA on NZVI focus on the reactivity of NZVI. This research will address the effects size fractioned Humic Acid has on the stability of NZVI.

2. Materials and Methods

2.1 NZVI Synthesis and Characterization

Nanosized zero valent iron was synthesized using green tea and ferrous sulfate heptahydrate ($FeSO_4 \cdot 7H_2O$) solution. synthesized through a green single-step synthesis using tea (*Camellia sinensis*) polyphenols (Hoag, Collins et al. 2009). Briefly green tea leaves were soaked in nitrogen purged water at a ratio of 3g to 50ml at 80°C for one hour. The tea leaf solution was then vacuum filtered through a 0.22mm filter and stored at 4°C when necessary. The ferrous sulfate heptahydrate solution was prepared in a glove bag to prevent oxidation. $FeSO_4$ solution was prepared using nitrogen purged water and the tea extract solution filtered a second time with a 0.22mm filter, was added to the $FeSO_4$ solution at a ratio of 2:1, one drop at a time, while the mixture was constantly being mixed. Upon the completion of tea extract solution addition, the mixture was stirred for 30 minutes, centrifuged at 20,000g for 15 minutes, rinsed with nitrogen purged water, and then centrifuged again at the same rate for the same time. The concentration of the NZVI suspension was determined through measuring iron concentrations for the thoroughly digested NZVI suspension samples. A portion of the NZVI was dried with nitrogen and characterized using a Burker D8 discover X-ray Diffractometer with Cu Ka radiation (λ= 1.5418 Å). Scanning electron microscopy (SEM) was used to determine the shape and morphology of NZVI using a Hitachi Model S4800 (operated at 5.0 kV and 10 μA).

2.2 Humic Acid Preparation and Characterization

The humic acid used for this research was purchased from Alfa Aesar (Tewksbury, MA). The humic acid received was dissolved in NanoPure water (specific resistivity ≥ 18.2 MΩ/cm), and the pH was adjusted using NaOH solution to ~7.0. Following filtration using 0.22mm filter

to remove any particulate matter, the humic acid solution was size-fractioned based on molecular size: < 3kDa, 3-10kDa, 10-100kDa, and >100kDa using Spectrum Labs™ dialysis membranes (Spectrum Chemical MFG Corp, New Brunswick, NJ). The concentration of dissolved organic carbon (DOC, in mg-C/L) in these different humic acid fractions was determined using a TOC analyzer (TOC-L analyzer, Shimazu, Japan).

To characterize the different size fractions of the humic acid, the UV-visible absorption spectra of the fractioned humic acid were obtained using an Agilent 8453 UV-visible spectrophotometer (Santa Clara, CA). The absorbance at 254 nm (A_{254}), normalized by the light path length (l) were used to calculate the chromophoric dissolved organic matter (CDOM) absorption coefficient at 254 nm, a_{254} (in m^{-1}), using the following equation (Lin and Guo 2020):

$$a_{254} = 2.303 \times A_{254}/l \quad (1)$$

To assess the aromaticity of the fractioned humic acid, specific UV absorbance at 254 nm ($SUVA_{254}$, in L/mg/m) was determined as (Weishaar, Aiken et al. 2003, Lin and Guo 2020):

$$\mathrm{SUVA_{254}} = \frac{\mathrm{A_{254}}}{\mathrm{DOC}(\frac{\mathrm{mg}}{\mathrm{L}})} \quad (2)$$

Fluorescence excitation-emission matrix (EEM) has also been widely used to characterize natural organic matter. In this research, spectra were gathered at 2 nm increments with scanning emission (Em) spectra from 240 to 600 nm by varying the excitation (Ex) at 5 nm increments from 220 to 480 nm on a spectrofluorometer (Fluoromax-4, Horiba Jobin Yvon, Edison, NJ). Before sample analysis, a blank scan was preformed using ultrapure water. Inner-filtering effects were minimized by dilution of samples. Subsequently, the humification index (HIX), an indicator for degree of humification of DOM, was computed at excitation wavelength of 254 nm as the ratio of Em intensity of 435-480 nm to the sum of Em intensity in the 300-345 and 435-480 nm (Dong, Wan et al. 2017, Xu and Guo 2017).

2.3 Stability and Aggregation Kinetics Measurements

For this research, the solution of fractioned humic acid (5 mM carbon) was mixed with NZVI (25 ppm Fe) for 24 hours to prepare humic acid coated NZVI, which was then stored in dark at 4°C. The coated NZVI suspensions were diluted to NaCl or $CaCl_2$ solutions that were purged with N_2 for 20 minutes and sonicated for 2 minutes. The NZVI concentration in the diluted solutions was 5 mg/L Fe. The stability and aggregation kinetics of coated NZVI suspended in various chemical solutions were measured through dynamic light scattering using a Zetasizer (Malvern Panalytical, Westborough, MA). The early-stage aggregation kinetics could be estimated from the initial rate of increase in the hydrodynamics radius (r) of the NZVI, which in turn is proportional to initial aggregation rate constant, k_{11}, as well as initial NZVI concentration (Chen and Elimelech 2006, Chen, Mylon et al. 2006):

$$K_A = \left(\frac{\mathrm{dr(t)}}{\mathrm{dt}}\right)_{\mathrm{t}\to 0} \propto \mathrm{k_{11}N_0} \qquad (3)$$

When different electrolyte (e.g., NaCl or $CaCl_2$) concentrations were used, a maximum value of NZVI aggregation kinetics could be reached at a threshold electrolyte value. In terms of NZVI aggregation, the condition above this threshold electrolyte concentration is often referred to as "favorable" condition in the sense that the chemical conditions were considered to favor maximum NZVI aggregation. The aggregation attachment efficiency, α_A, could be calculated as

$$\alpha_{\mathrm{A}} = \frac{\mathrm{k_{11}}}{(\mathrm{k_{11}})_{\mathrm{f}}} \qquad (4)$$

To determine the stability of the NZVI the slope was calculated from slope of the size-time data for each humic acid fractionation, and the average was taken of the replicate sets of NZVI size evolution data.

2.4 Particle-Particle Energy Interactions

The stability and aggregation behavior of NZVI are strongly dependent on the particle-particle energy interactions, which in turn is influenced by factors such as water chemistry conditions (e.g., ionic strength and ion types). When there exist strong repulsive energy interactions between the NZVI particles, the NZVI suspension will tend to remain stable with minimal aggregation and size growth. In contrast, if the energy interactions between the NZVI particles are attractive, there will be substantial aggregation and size increase.

In this research, the energy interactions between the NZVI particles were estimated using the extended DLVO (xDLVO) theory, which assumes that the total energy interactions between the NZVI particles are the summation of the Lifshitz−van der Waals (LW) interaction, the electrostatic double layer (EDL) interaction and the Lewis acid-base (AB) interaction, which includes hydrogen-bonding interactions (van Oss, Docoslis et al. 1999, Wu and Nancollas 1999, van Oss and Giese 2003, van Oss 2007, van Oss 2008):

$$\Phi^{\text{total}} = \Phi^{\text{LW}} + \Phi^{\text{EDL}} + \Phi^{\text{AB}} \qquad (5)$$

The LW interaction includes (1) the randomly oriented permanent dipole-permanent dipole interaction (i.e., the orientation interaction), (2) the randomly oriented permanent dipole-induced dipole interaction (i.e., the induction interaction) and (3) the fluctuating dipole-induced-dipole interaction (i.e., the dispersion interaction) (van Oss, Giese et al. 1990). The LW interactions are usually attractive and decay rapidly with separation distance. For the NZVI-NZVI (sphere-sphere geometry) system the LW interaction energies (Φ^{LW}) can be calculated using the following equation (Israelachvili 1991):

$$\Phi^{\text{LW}} = -Aai12h \qquad (6)$$

where a_i is the radius of the NZVI particle; h is the separation distance between the NZVI particles and A is the Hamaker constant. In general, the Hamaker constant can be calculated from the LW surface tension parameters of material 1 (γ_1^{LW}), liquid (γ_L^{LW}) and material 2 (γ_2^{LW}) (van Oss, Giese et al. 1990, Wu and Nancollas 1999):

$$A = 24\pi h_0^2 \left(\sqrt{\gamma_1^{LW}} - \sqrt{\gamma_L^{LW}}\right)\left(\sqrt{\gamma_2^{LW}} - \sqrt{\gamma_L^{LW}}\right) \quad (7)$$

where h_0 represents the minimum equilibrium distance between the surfaces due to Born repulsion and equals to 0.157nm. If material 1 and material 2 are the same (e.g., NZVI) and liquid is water, equation (6) can be written as:

$$A = 24\pi h_0^2 \left(\sqrt{\gamma_i^{LW}} - \sqrt{\gamma_w^{LW}}\right)^2 \quad (8)$$

where γ_i^{LW} is the LW surface tension of NZVI and γ_w^{LW} is LW surface tension of water and equals to 21.8 mJm^{-2}. γ_i^{LW} can be estimated from the measurement of contact angles of polar and nonpolar liquids (see below).

The surface of the NZVI particles are charged, but the surface potential associated with such charges cannot be directly measured due to the presence of bound counter-ions and water molecules, which is often referred to as Stern layer or inner-Helmholtz plane (van Oss, Giese et al. 1990). Right next to the Stern layer toward the bulk solution exists another layer of hydrated counter ions as well as water molecules, which is commonly referred to as outer Helmholtz plane. Further away from the outer Helmholtz plane is the slipping plane which separates the particle (with the bound water molecules and counter ions) and the bulk solution. The potential of the slipping plane can be measured through determining the velocity of the particles within an applied electric field and is referred to as zeta (ξ) potential.

In this research, the zeta potential of the NZVI was measured using a Zetasizer (Malvern Analytical, Westborough, MA). The electrostatic double layer interaction between two particles of similar sizes can be calculated from the measured zeta potential (ξ) values as (Israelachvili 1991, Elimelech, Gregory et al. 1998):

$$\Phi^{\mathrm{EDL}} = \pi\varepsilon_0\varepsilon_w a_i \xi^2 \left\{ ln\left[\frac{1+\exp(-\kappa h)}{1-\exp(-\kappa h)}\right] + ln[1-\exp(-2\kappa h)] \right\} \qquad (9)$$

where ε_0 and ε_w are the dielectric permittivity of vacuum and water, respectively; κ is the inverse of the Debye length and is given by:

$$\kappa = \sqrt{\frac{2e^2 N_A I}{\varepsilon_r \varepsilon_0 k_B T}} \qquad (10)$$

where *e* is the charge of the electron; *I* is the ionic strength of the electrolyte in $\frac{M}{m^3}$; ε_0 is the permittivity of free space; ε_r is the dielectric constant; k_B is the Boltzmann constant; *T* is the absolute temperature in kelvins; N_A is the Avogadro number. For specific electrolytes, the inverse of Debye length can be simplified to (Israelachvili 1991):

$$\kappa = \begin{cases} \frac{\sqrt{[\mathrm{NaCl}]}}{0.304}\ nm^{-1}, \text{1: 1 electrolyte, such as NaCl} \\ \frac{\sqrt{[\mathrm{CaCl_2}]}}{0.176}\ nm^{-1}, \text{1: 2 electrolyte, such as } \mathrm{CaCl_2} \end{cases} \qquad (11)$$

The decay of Lewis acid-base interaction energy (Φ^{AB}) between two presumably spherical particles at different separation distances is calculated as (van Oss, Giese et al. 1990, Wu and Nancollas 1999):

$$\Phi^{AB} = \pi a_i \lambda_w \Delta G_{h_0}^{AB} e h 0 - h \lambda w \qquad (12)$$

where λ_w (=0.6 nm) is the characteristic decay length of AB interactions in water; and $\Delta G_{h_0}^{AB}$ represents the hydrophobicity interaction free energies per unit area corresponding to h_0. The

value of $\Delta G_{h_0}^{AB}$ between 2 NZVI particles can be calculated from the electron-acceptor (γ^+) and electron-donor (γ^-) surface tention parameters of NZVI and water:

$$\Delta G_{h_0}^{AB} = -4\left(\sqrt{\gamma_i^+\gamma_i^-} + \sqrt{\gamma_w^+\gamma_w^-} - \sqrt{\gamma_i^+\gamma_w^-} - \sqrt{\gamma_w^+\gamma_i^-}\right) \quad (13)$$

where γ_i^+ and γ_i^- are the electron-acceptor and electron-donor surface tention parameters for NZVI, and γ_w^+ and γ_w^- are the electron-acceptor and electron-donor surface tention parameters for water, both of which equal to 25.5 mJ m^{-2}.

The calculation of the Hamaker constant, *A*, and $\Delta G_{h_0}^{AB}$ requires the surface tension parameters of γ_i^{LW}, γ_i^+ and γ_i^- for the NZVI. For this purpose, the NZVI suspensions were placed on clean glass lides, dried in a glovebag for 24 hours, and the contact angles (Θ) of three probing liquid, diiodomethane, glycerol and DI water, on the dried layers of NZVI were measured using a Rame-Hart goniometer (Wang, Xu et al. 2011). Briefly, for each type of NZVI, five drops of the probing liquid were placed (not in contact with one another) on the surface of the dried NZVI and ten measurements were taken for each drop. An average was then taken of all 50 measurements. Based on the Young-Dupré equation, the values of γ_i^+, γ_i^- and γ_i^{LW} and the corresponding values of the probing liquids were related to the measured contact angle values (van Oss, Giese et al. 1990):

$$\gamma_L^L(1+\cos\Theta) = 2\sqrt{\gamma_L^{LW}\gamma_i^{LW}} + 2\sqrt{\gamma_L^+\gamma_i^-} + 2\sqrt{\gamma_L^-\gamma_i^+} \quad (14)$$

where the subscript *i* represents NZVI, and the subscript *L* represents glycerol (γ^L=64.0, γ^{LW} = 34.0, γ^+3.92, γ^-=57.4 mJ m^{-2}), diiodomethane (γ^L= 50.8, γ^{LW}= 50.8 and γ^+= γ^-= 0 mJ m^{-2}) or water (γ^L=72.8, γ^{LW}=21.8 and γ^+ = γ^-=25.5 mJ m^{-2}), respectively. With the three probing liquids, the values of γ_i^+, γ_i^- and γ_i^{LW} can be obtained using equation 14.

3. Results and Discussion

3.1 XRD and SEM image

The NZVI synthesized using green tea and ferrous sulfate heptahydrate was 200-300 nm in size and unoxidized (Figure 1). The XRD data presented no distinctive peaks on the spectra which indicated that the NZVI had an amorphous structure and was not crystalline in nature. Synthesis of amorphous NZVI using leaf extracts of different plants such as eucalyptus, mulberry, pomegranate, and cherry has been reported (Kheshtzar, Berenjian et al. 2019). The presence of organic material from leaf extract responsible for stabilizing and capping the NZVI was proposed to be the cause of the broad shoulder peak of 2θ vaules from 20° to 30° (Wang et al., 2014). The secondary peak appearing at around 2θ of 44-45° is considered as indicative peak for NZVI by some researchers (Wang et al., 2014, Kuang et al., 2013).

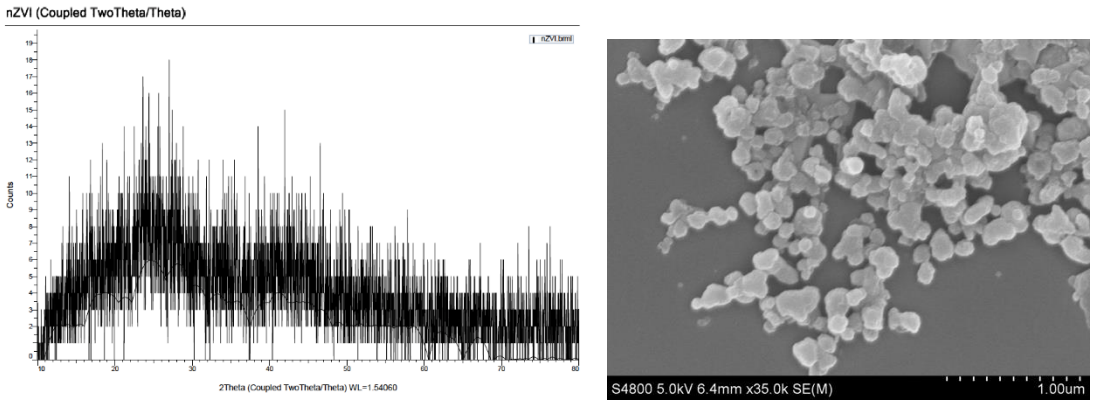

Figure 1. XRD result of the NZVI (left panel) and SEM image of NZVI (right panel).

3.2 Humic Acid Characterization

The absorption coefficient at 254 nm, a_{254}, of the size-fractioned ranged from 3.9 to 22 m^{-1} (Table 1). The a_{254} value was significantly lower for the <3 kDa fraction, increased to 15.0 m^{-1} for the 3-10 kDa fraction, and to 22.0 m^{-1} for the 10-100 kDa fraction and leveled off for the >100 kDa fraction. This result is consistent to findings from previous studies which showed that the values of a_{254} decreased with the degradation of natural humic acid (Dziedzic, Wodka et al. 2010). Additionally, the observed values of $SUVA_{254}$, which reflects aromaticity, increased with the humic acid sizes (Table 1), suggesting that humic acid fractions with larger molecular sizes were associated with greater aromatic content (Weishaar, Aiken et al. 2003, Hansen, Kraus et al. 2016). It was reported that the values of HIX increases from fresh plant materials (~1.3) to soil soluble dissolved organic matter (~5.2) to lower-molecular-weight fulvic acid (~15.9) (Ohno 2002). The observe HIX values (Table 1) generally increased from high-molecular-weight humic acid fractions to low-molecular-weight humic acid fractions as humification represents a process of continuous organic matter degradation. The measured optical spectra properties of the humic acid (without any size fractionation) generally reflect the average of the different size-fractions.

Table 1. Results of humic acid characterization.

	a_{254} (m^{-1})	$SUVA_{254}$ (L/mg-C/m)	HIX
<3 kDa	3.9	1.71	7.7
3-10 kDa	15.0	6.50	19.9
10-100 kDa	22.0	9.55	6.8
>100 kDa	21.2	9.20	2.1
Whole humic acid	20.3	8.83	5.5

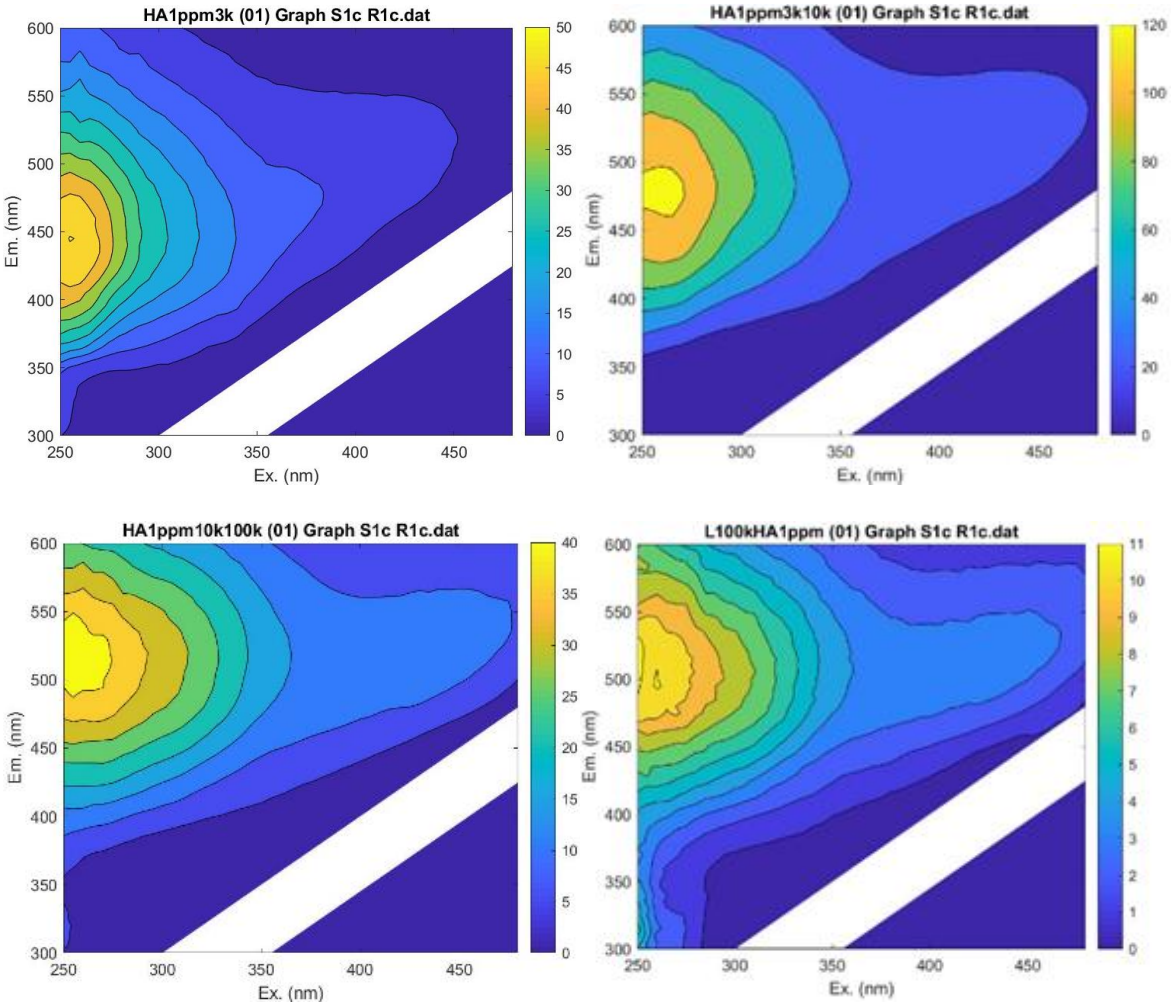

Figure 2. Fluorescence excitation–emission matrix (EEM) spectra of different size fractions of the humic acid.

EEM spectra from the whole and size-fractionated humic acid samples showed that they have different Ex/Em peak locations (Figure 2). Notably the peaks that are associated with protein-like structures (e.g., Ex/Em = 205/305 nm) were absent from the EEM spectra. For the <3 kDa fraction, the Ex/Em peak locations were ~255/445 nm, which is often referred to as peak A (Stubbins, Lapierre et al. 2014, Hansen, Kraus et al. 2016). Humic acid with this EEM spectra feature tends to exhibit low biolability but high photolability (Stubbins, Lapierre et al. 2014). With the increase in molecular weight, the excitation peak remained virtually unchanged (~255

nm), but the emission peak increased from ~445 nm to 520 nm (Figure 2). The redshift in the EEM specta is consistent with the increase in humic acid molecular weight. These peaks were considered as shoulders of peak A, and reflected highly-processed, terrigenous humic acid (Stubbins, Lapierre et al. 2014).

3.3 Stability and Aggregation Kinetics of NZVI

The effects of fractioned humic acid coating on the stability of NZVI were evaluated under two different water chemistry conditions, where either NaCl (1:1 electrolyte) or $CaCl_2$ (1:2 electrolyte) were used. The preliminary results showed that NZVI (coated or uncoated) were stable over long period of time when NaCl concentrations were below 100 mM. The stability and aggregation of NZVI (coated or uncoated) were evaluated using NaCl concentrations that were 100 mM or higher, and examples results are shown in Figure 3. The effects of NaCl concentrations and the fractioned humic acid coating on the stability and aggregation kinetics of the NZVI were clear from Figure 3. For the uncoated NZVI, the particles were stable with the presence of 100 mM NaCl. At NaCl concentrations higher than 100 mM, the size of the NZVI increased linearly with time and faster aggregation kinetics were generally associated with higher NaCl concentrations. When the NZVI were coated with <3 k Da humic acid, they remained stable under the presence of 200 mM NaCl. Further increase in NaCl concentration led to aggregation of the coated NZVI. Similar trend was observed for the coating of NZVI using other fractioned humic acid, although the stabilizing effects seemed to decrease with increase in the fractioned humic acid sizes.

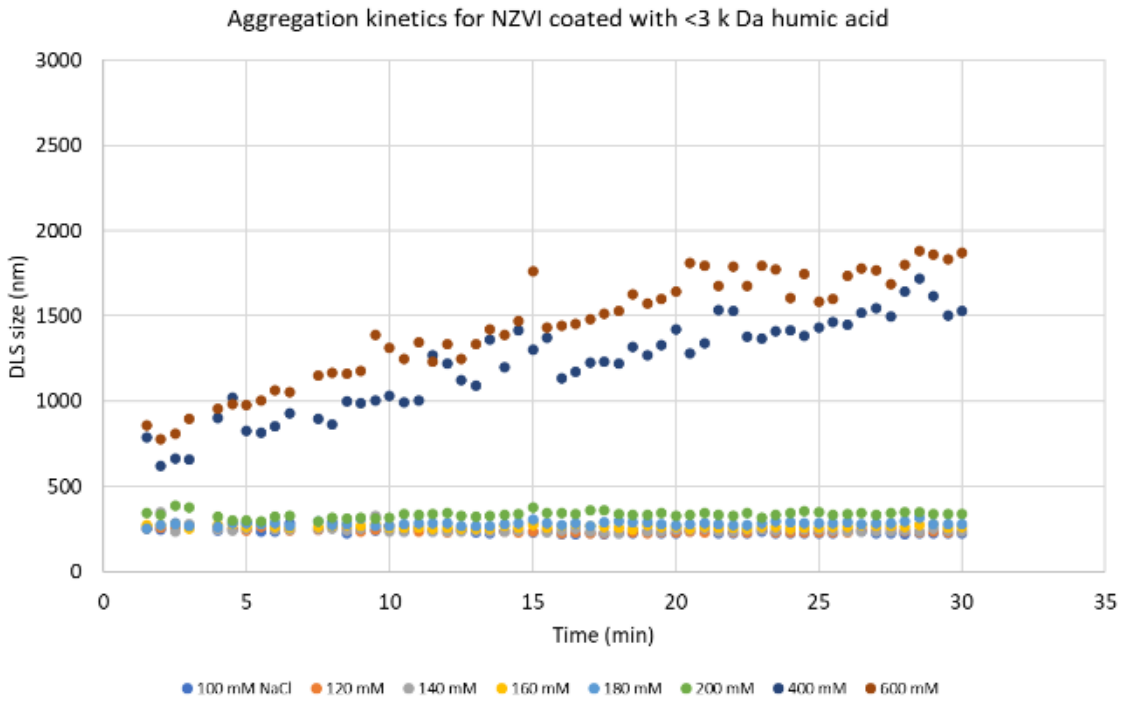
Aggregation kinetics for NZVI coated with <3 k Da humic acid
DLS size (nm)
Time (min)
100 mM NaCl
120 mM
140 mM
160 mM
180 mM
200 mM
400 mM
600 mM

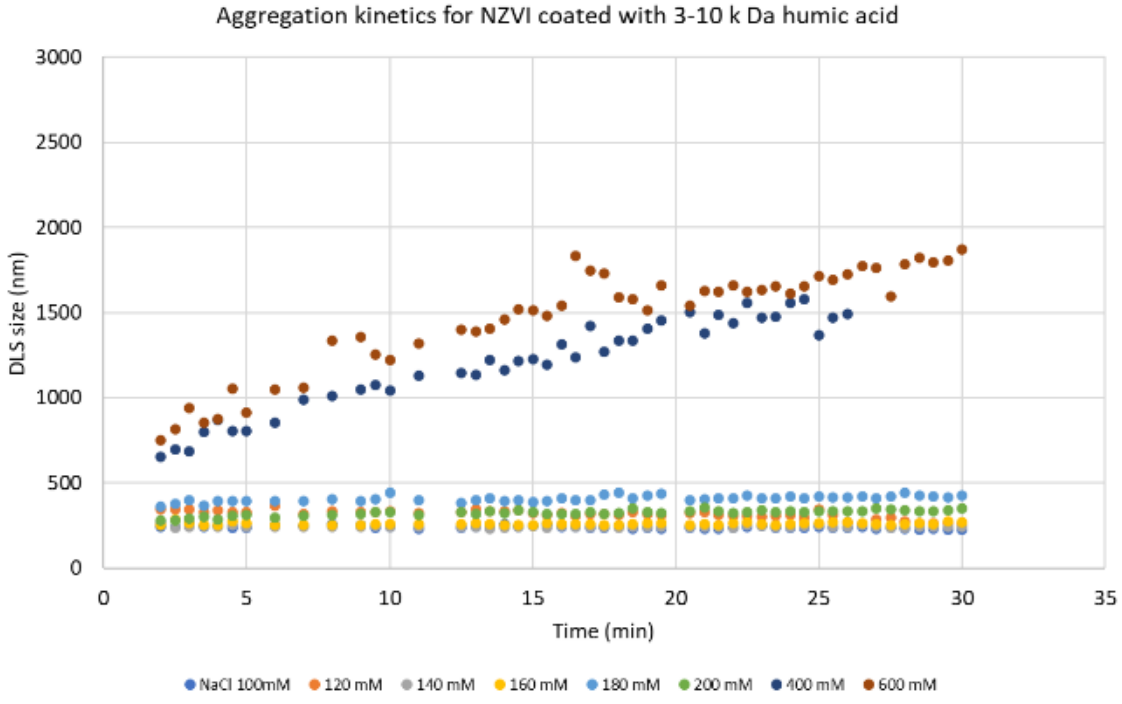
Aggregation kinetics for NZVI coated with 3-10 k Da humic acid
DLS size (nm)
Time (min)
NaCl 100mM
120 mM
140 mM
160 mM
180 mM
200 mM
400 mM
600 mM

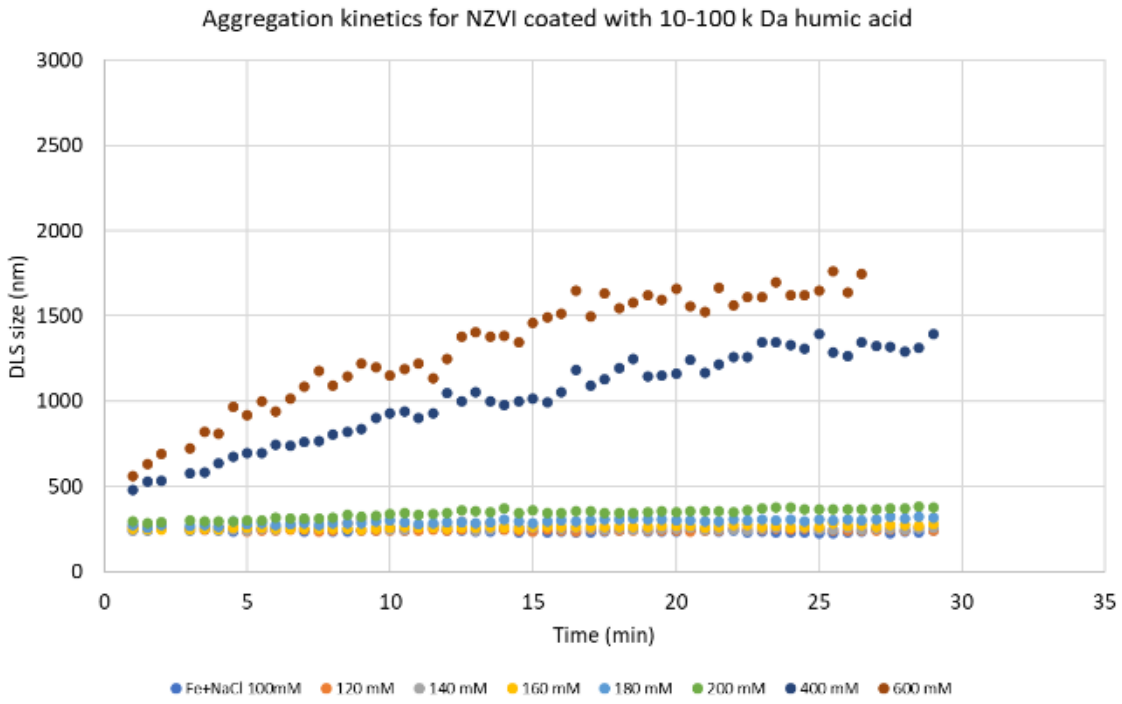
Aggregation kinetics for NZVI coated with 10-100 k Da humic acid
DLS size (nm)
Time (min)
Fe+NaCl 100mM
120 mM
140 mM
160 mM
180 mM
200 mM
400 mM
600 mM

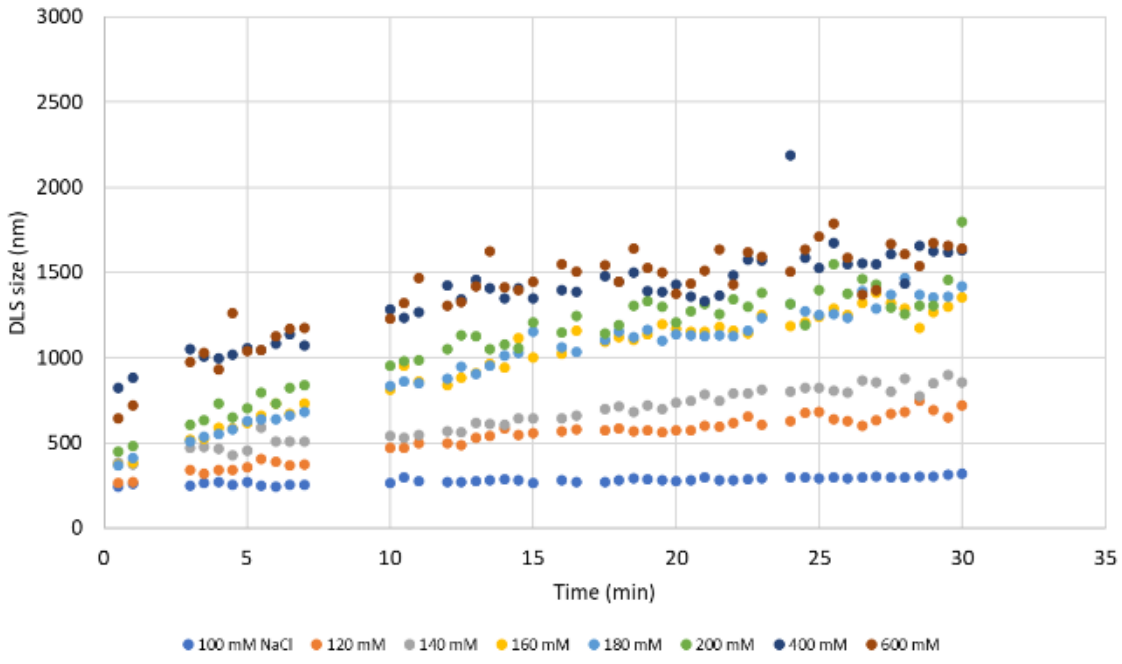
Aggregation kinetics for NZVI coated with >100 k Da humic acid
DLS size (nm)
Time (min)
100 mM NaCl
120 mM
140 mM
160 mM
180 mM
200 mM
400 mM
600 mM

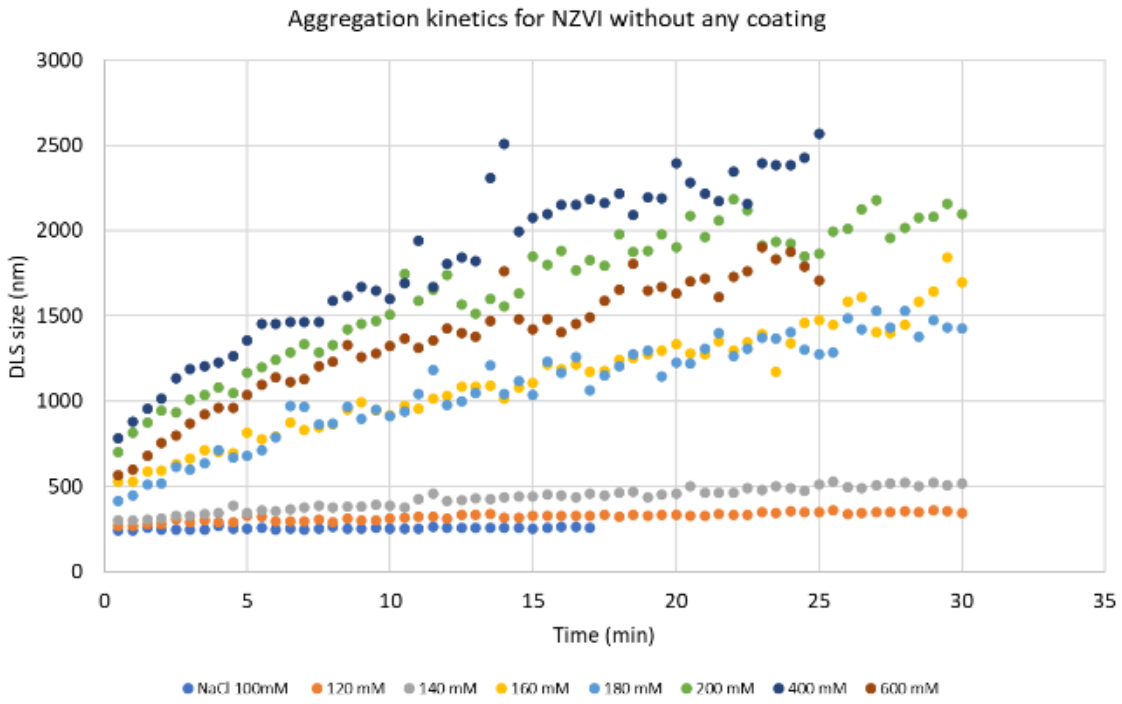

Figure 3. Example DLS measurement results for NZVI with and without humic acid coating.

The NZVI aggregation kinetics were fitted to equation (3) and it was observed that the values of k_{11} reached a plateau value under high NaCl concentrations (e.g., >1000 mM). The values of k_{11} under favorable conditions (maximum aggregation kinetics) were identified and the aggregation attachment efficiency, α_A, were calculated using equation (4), and the results are presented in Figure 4. Please note that if the NZVI particles were stable when suspended in a NaCl solution (flat size line), the slope of the size vs time line were practically zero (or slight negative). As a result, the values of the aggregation attachment efficiency were effectively zero and could not be shown in Figure 4. For instance, no data were available for α_A when NZVI coated with <3 k Da HA were suspended in 100 mM NaCl.

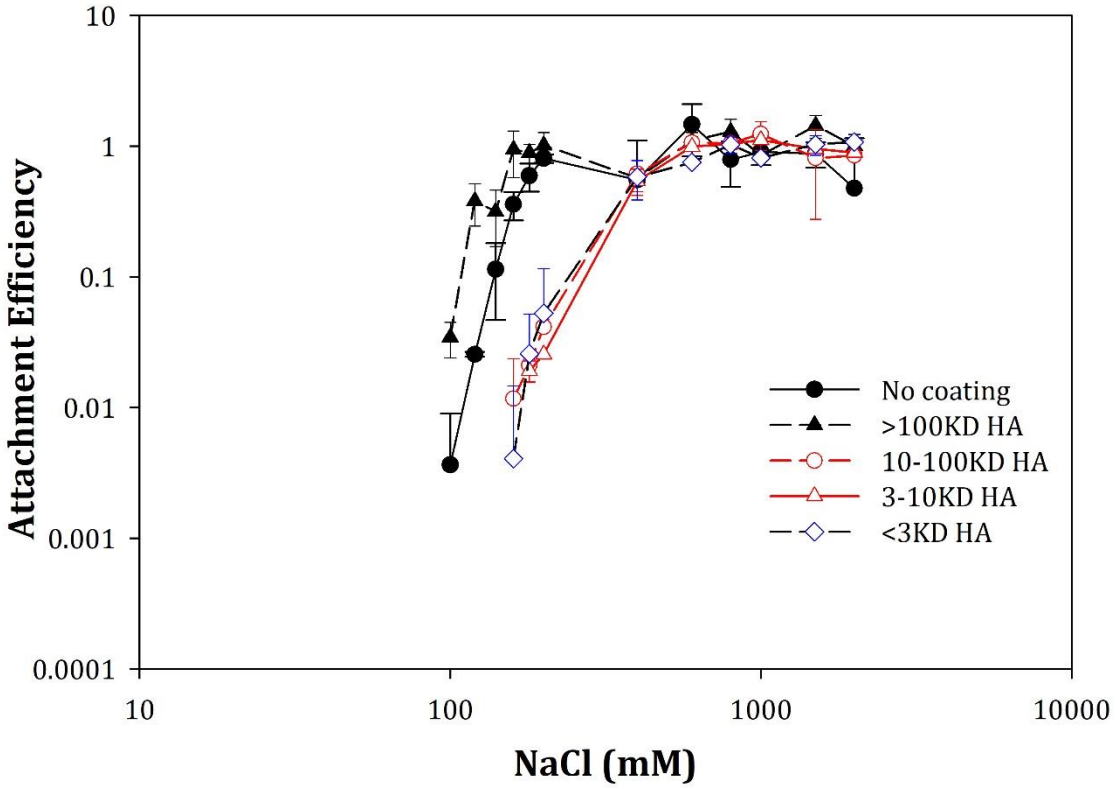

Figure 4. The aggregation attachment efficiency, α_A, for coated and uncoated NZVI under different NaCl concentrations.

Results shown in Figure 4 summarized the major effects of humic acid coating (fractioned or whole) on NZVI stability. The coating of 3 sizes fractions of humic acid (i.e., <3 k Da, 3-10 k Da and 10-100 k Da) significantly increased the stability of the NZVI when NaCl concentration was below 600 mM. When NaCl concentration reached 600 mM or above, the aggregation kinetics for both coated and uncoated NZVI plateaued.

$CaCl_2$, however, was significantly more effective in promoting the aggregation of the NZVI. Therefore, based on results of preliminary investigations, the concentration range of $CaCl_2$ was 2 mM to 15 mM. Example results of NZVI (coated or uncoated) aggregation when

suspended in $CaCl_2$ are shown in Figure 5. Consistent to the results observed in NaCl solutions, NZVI were stable under low concentrations of $CaCl_2$ conditions. For instance, there was no observable increase in NZVI sizes when they were suspended in ≤3 mM $CaCl_2$. Further increases in $CaCl_2$ concentrations generally led to increasingly more rapid NZVI aggregation.

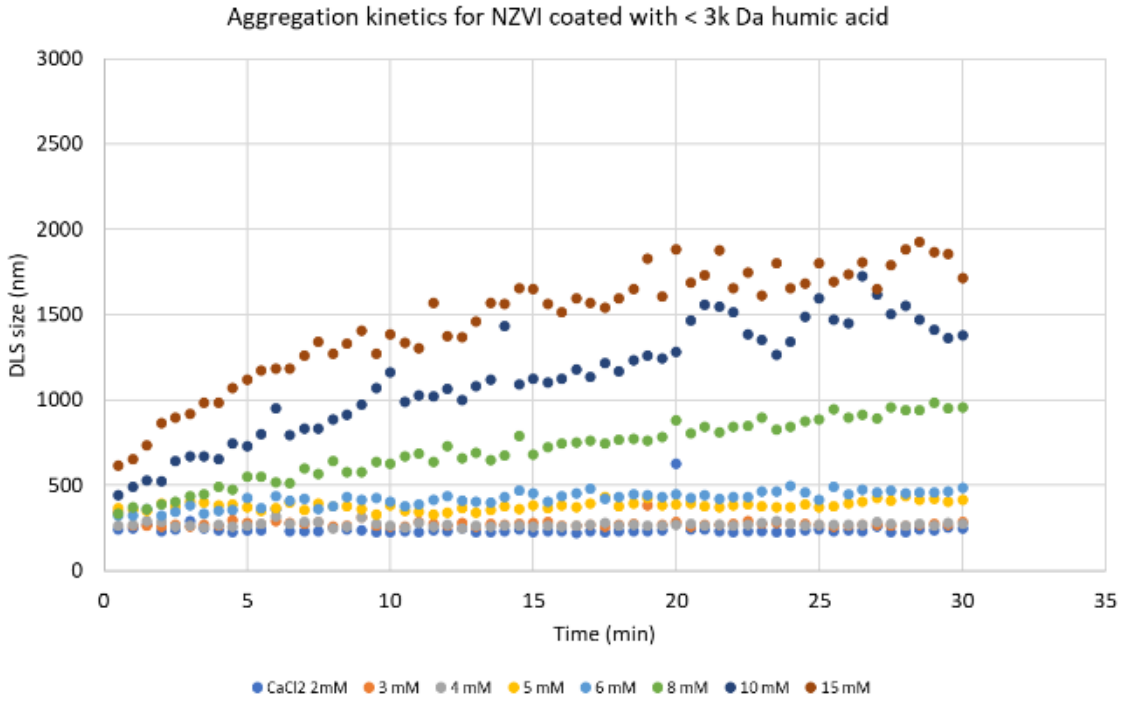

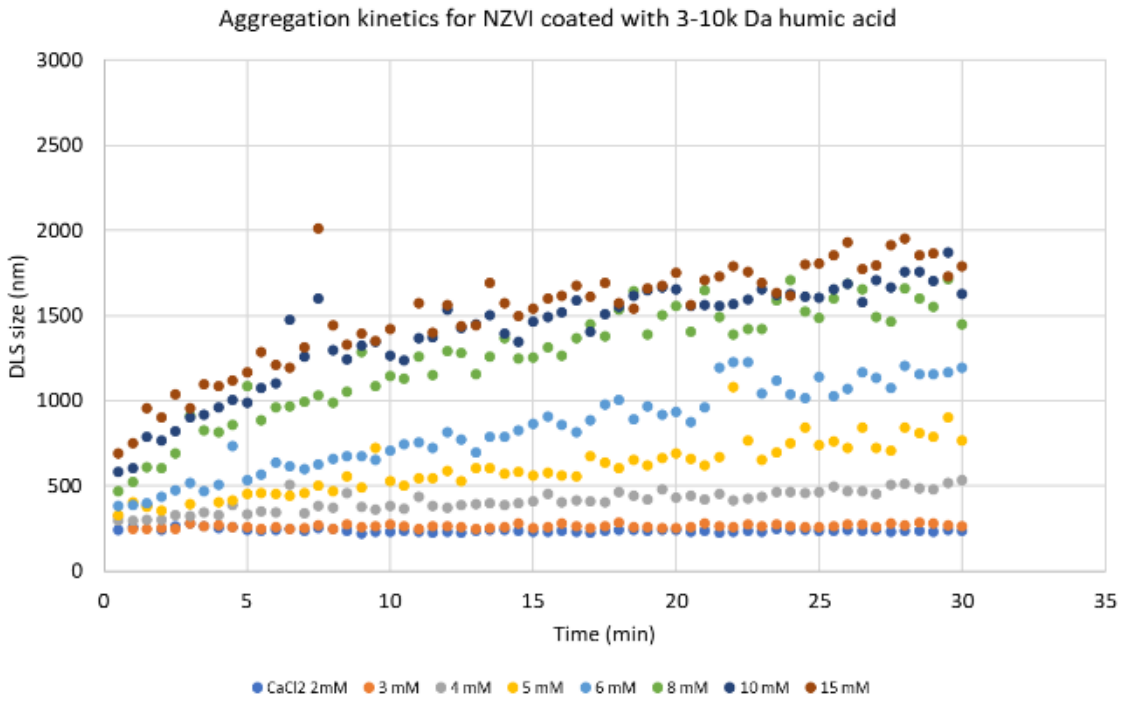
Aggregation kinetics for NZVI coated with 3-10k Da humic acid
DLS size (nm)
Time (min)
CaCl2 2mM
3 mM
4 mM
5 mM
6 mM
8 mM
10 mM
15 mM

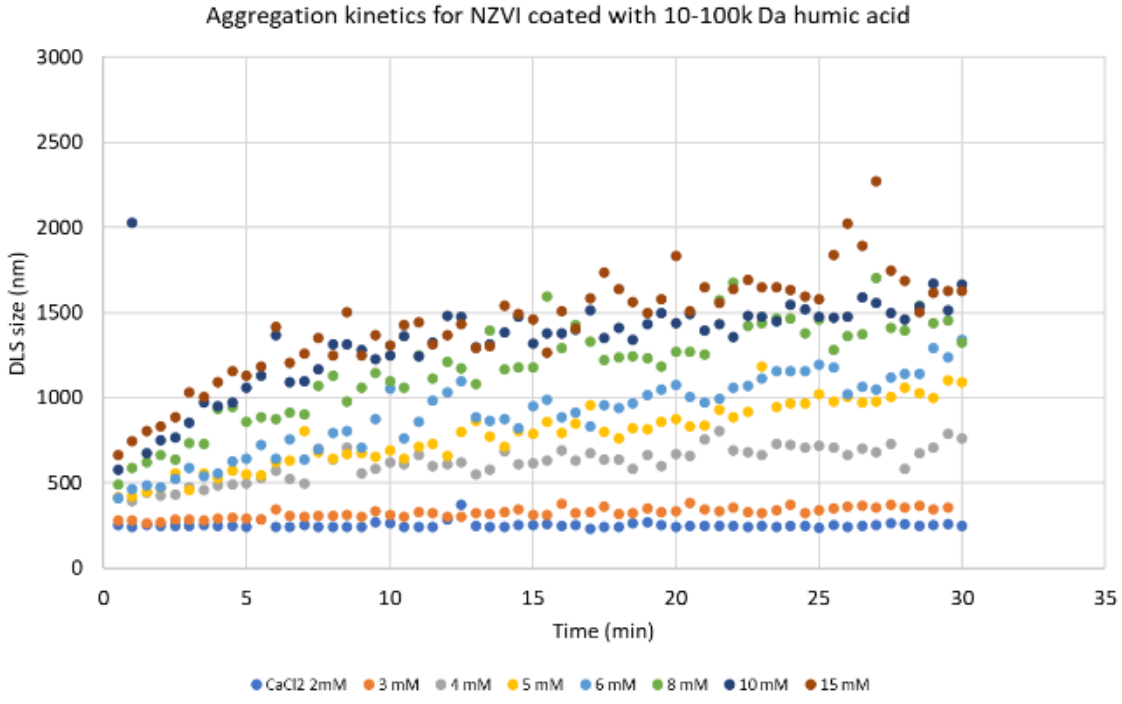
Aggregation kinetics for NZVI coated with 10-100k Da humic acid
DLS size (nm)
Time (min)
CaCl2 2mM
3 mM
4 mM
5 mM
6 mM
8 mM
10 mM
15 mM

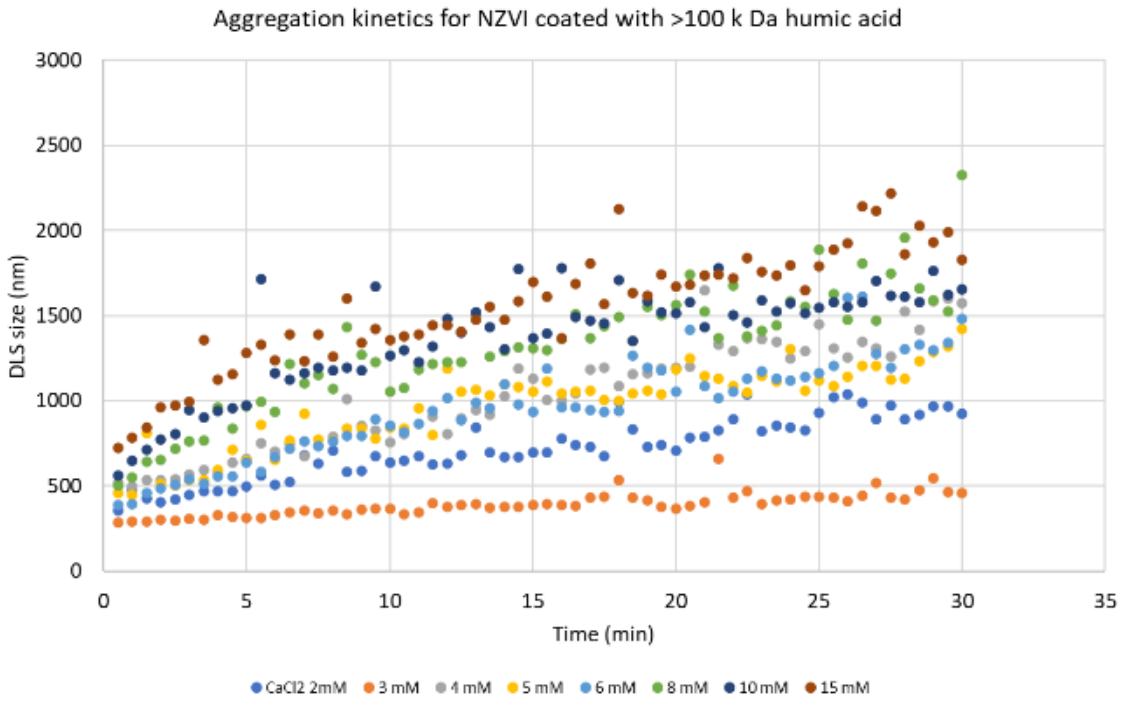

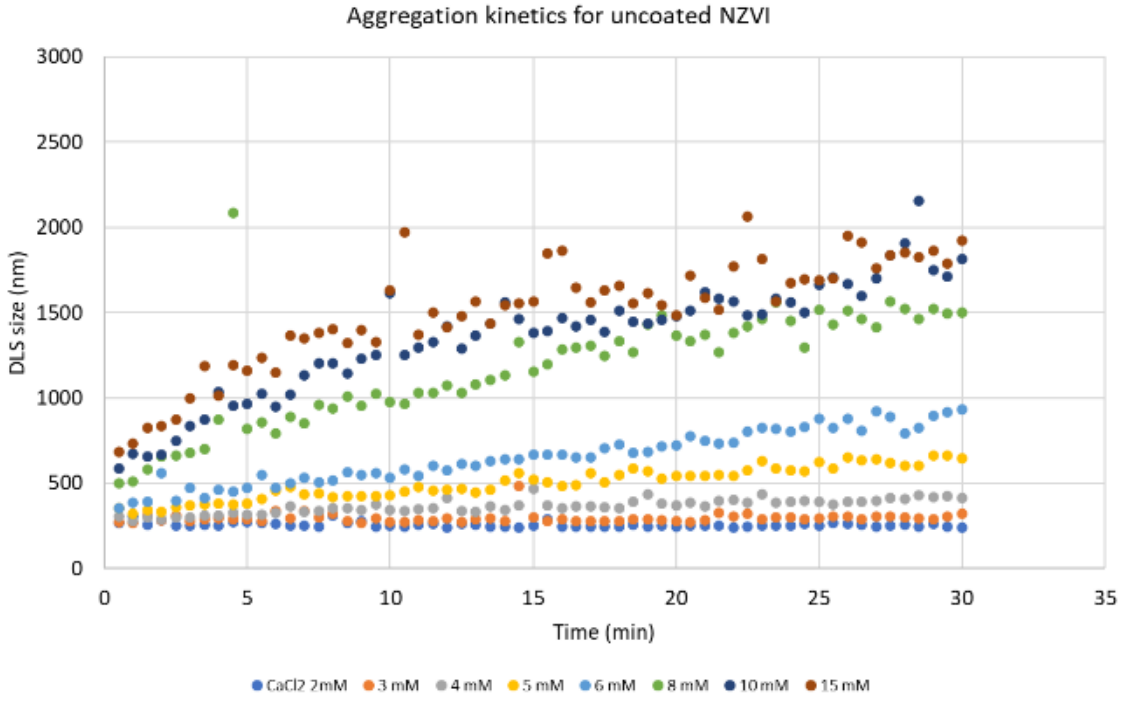

Figure 5. Example DLS measurement results for NZVI with and without humic acid coating.

The fitting of the NZVI aggregation data to equation (3) and the subsequent analysis using equation (4) could allow us to estimate aggregation attachment efficiency, α_A, under the presence of $CaCl_2$ (Figure 6). As the coating using <3 k Da humic acid led to enhanced stability (and lower aggregation kinetics) of NZVI, such stabilizing effects were not observed for the other size fractions of humic acid. Rather, NZVI coated with 10-100 k Da and >100 k Da humic acid fractions displayed faster aggregation kinetics (Figure 6).

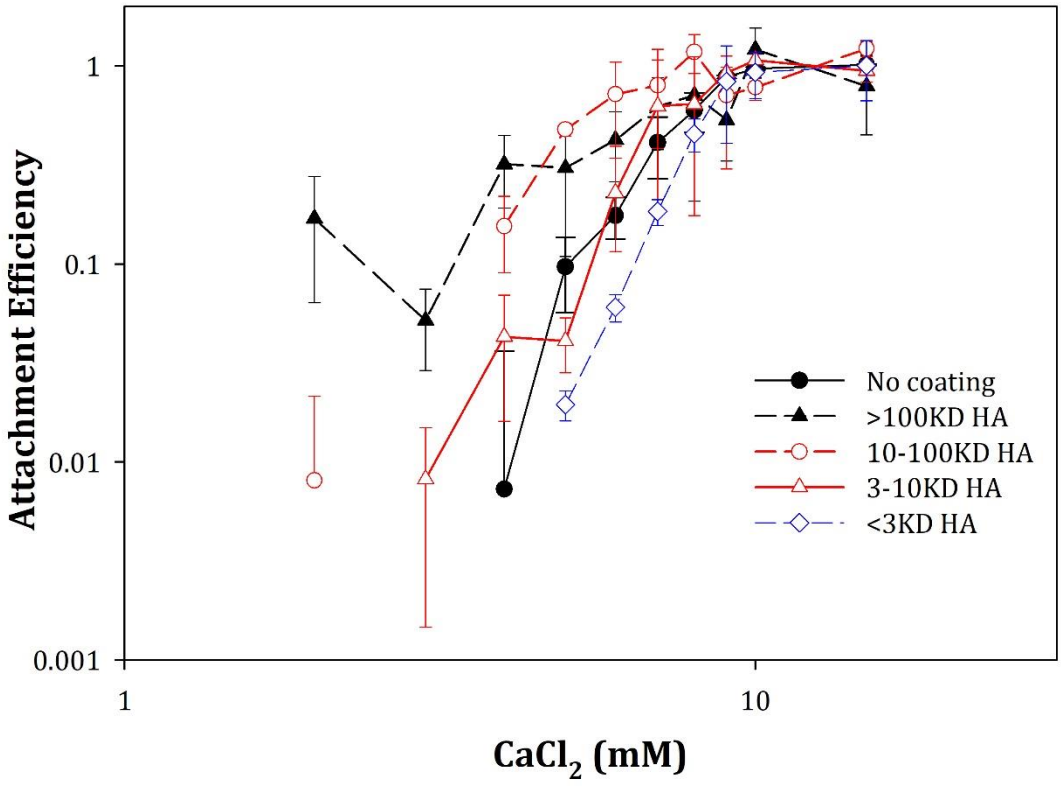

Figure 6. The aggregation attachment efficiency, α_A, for coated and uncoated NZVI under different $CaCl_2$ concentrations. Missing points indicated that the attachment efficiency could not be assessed because the fitted slope of the size vs. time line was practically zero or slightly negative.

In summary, results obtained in this research showed that 1) coating of NZVI with lower-molecular-weight humic acid enhanced their stability when suspended in NaCl or $CaCl_2$ solutions; 2) compared to NaCl, $CaCl_2$ could significantly lower the stability of NZVI, regardless of surface coating; 3) the stability of NZVI (coated and uncoated) decreased with increasing salt concentrations.

3.4 NZVI Interaction Energy Using XDLVO Theory

The coating of fractioned humic acid on the surface of NZVI affected NZVI's stability through changing the energy interactions between the NZVI particles. In this research, we applied the XDLVO theory to examine the particle-particle energy interactions.

The contact angles of 3 probing liquids, water, glycerol and diiodomethane on layers of coated and uncoated NZVI were measured using a goniometer (Table 2). The surface tension terms were calculated using equation 14. The Hamaker constant (A) and the standard hydrophobicity interaction free energies per unit area $\Delta G_{h_0}^{AB}$ were then calculated using equations (13) and (8) respectively. The calculated Hamaker constants varied from 5.69 to 7.19 ××10^{-21} J and the values of $\Delta G_{h_0}^{AB}$ ranged from 50.6 to 58.46 mJ m^{-2}, suggesting that the coating of NZVI did not lead to significant changes in liquid surface tensions.

Table 2. Measured contact angles of three probing liquids (polar: water and glycerol; nonpolar: diiodomethane) on thin layers of coated and uncoated NZVI. A minimum of 5 measurements were performed and the values in parenthesis represent the standard deviation. The Hamaker constant (A) and the standard hydrophobicity interaction free energies per unit area $\Delta G_{h_0}^{AB}$ were determined from the contact angle values.

		NoHA	>100kDaHA	10-100kDaHA	3-10kDaHA	<3kDaHA
Contact angle (deg)	water	29.36 (±4.26)	34.40 (±14.28)	27.24 (±3.26)	24.50 (±2.23)	29.07 (±2.40)
	glycerol	59.42 (±8.69)	63.99 (±6.04)	68.42 (±8.62)	65.20 (±6.41)	69.72 (±3.25)
	diiodomethane	32.54 (±1.55)	34.97 (±3.08)	36.79 (±3.69)	30.45 (±0.22)	31.38 (±3.68)
A (10^{-21} J)		6.70	6.13	5.69	7.19	6.98
$\Delta G_{h_0}^{AB}$ (mJ m^{-2})		54.00	50.60	58.46	57.97	53.95

The measured zeta potential values for both the coated and uncoated NZVI are shown in Figure 7. The humic acid coating caused significant changes in the zeta potential of the NZVI, particularly when suspended in NaCl solutions (Figure 7). For instance, on average, the zeta potential of the NZVI coated with <3 k Da humic acid was ~3.5 mM lower than those of the uncoated NZVI when they were suspended in NaCl solution. For other humic acid fractions, the differences were ranging from ~3.9 mM (3-10k Da fraction) to ~6.3 mM (10-100 k Da fraction) lower. It was also observed that the increase in NaCl or $CaCl_2$ concentration resulted in less negative zeta potential values for the coated and uncoated NZVI due to the suppression of the electrostatic double layer (Israelachvili 1991).

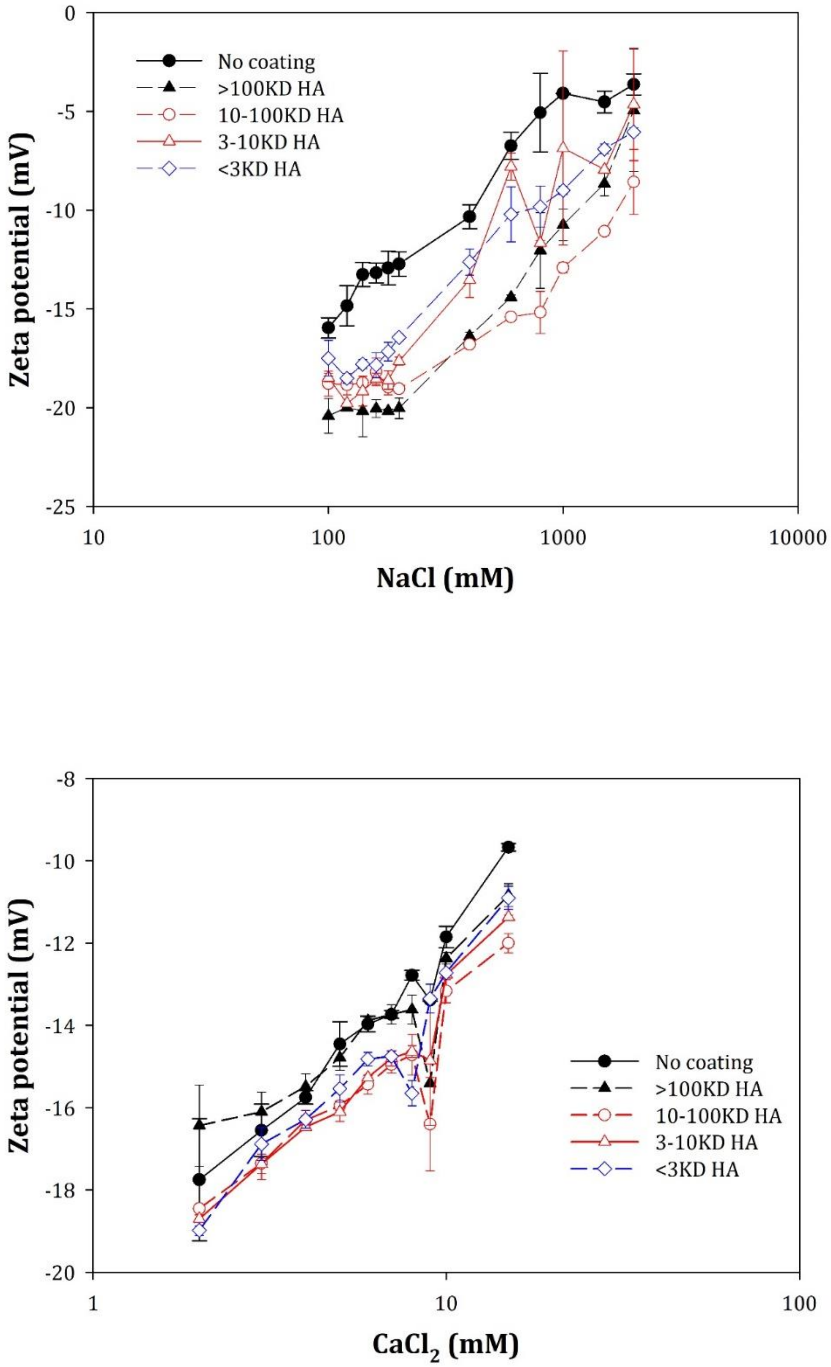

Figure 7. Measured zeta potential values of the coated and uncoated NZVI suspended in various concentrations of NaCl or $CaCl_2$.

The concentrations of $CaCl_2$ used in this research were 1-2 orders of magnitude lower than the concentrations of NaCl, but the measured zeta potential values of NZVI (coated and uncoated) suspended in both groups of solutions were comparable. The dramatic effects of divalent cations on the zeta potential values of the NZVI were partly related to the distribution of the cations at the surface of the particles (Israelachvili 1991). For instance, it was shown that for a particle with a surface potential of -100 mV, when suspended in 3 mM $CaCl_2$ solution, the Ca^{2+} concentration at the particle surface is 7 M. In contrast, when the same particle was suspended in 100 mM NaCl, the Na^+ concentration at the particle surface was only 5 M (Israelachvili 1991).

The particle-particle interaction energy profiles, which played critical roles in the stability and aggregation kinetics of the NZVI, were then calculated using Hamaker constant and $\Delta G_{h_0}^{AB}$ values presented in Table 2, zeta potential values presented in Figure 7 and the initial measurements of particle sizes. This led to the creation of a large number of interaction energy profiles. A few representative particle-particle interaction energy profiles are included here to reflect the general trend that was observed.

The LW interactions were attractive (negative values in the interaction energy profile), the EDL interactions were repulsive; and the AB interactions were also repulsive (Figures 8 and 9). All three interactions decayed rapidly but at different rates with the AB interactions decaying at the fastest rate. Overall, the EDL repulsion was one order of magnitude or more lower than the AB repulsion. As a result, the repulsive interaction between the NZVI (coated or uncoated) was dominated by the AB force. When combined, the XDLVO energy profiles showed significant barrier at <1nm for the formation of primary energy minimum (Figures 8 and 9). The magnitude of the energy barrier was *not* correlated with the observed stability and aggregation kinetics of the NZVI. For instance, the energy barriers for both the uncoated NZVI and the NZVI coated

with <3k Da humic acid were higher when they were suspended in 2000 mM NaCl than when they were suspended in 200 mM NaCl. Both types of NZVI exhibited stronger stability (and slower aggregation kinetics) under the presence of 200 mM NaCl.

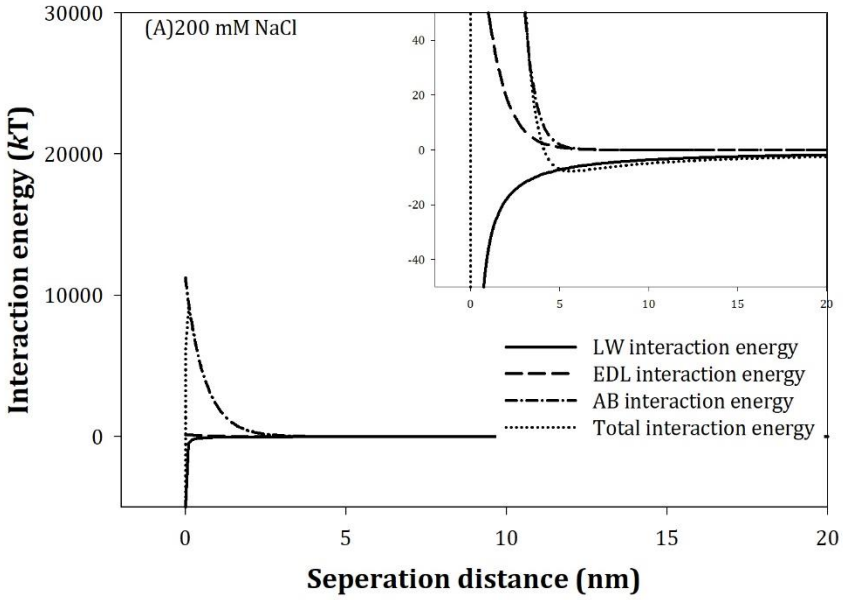

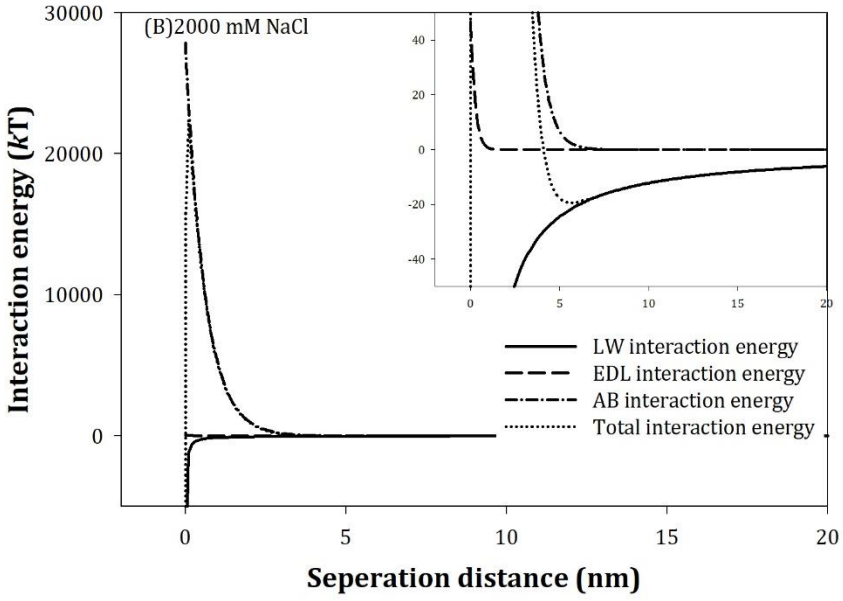
(B)2000 mM NaCl
Interaction energy (kT)
Seperation distance (nm)
LW interaction energy
EDL interaction energy
AB interaction energy
Total interaction energy

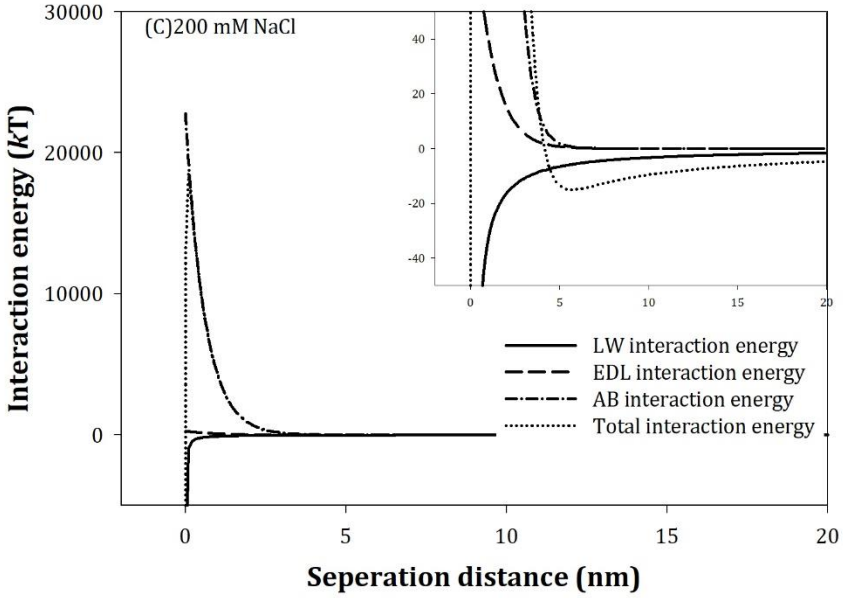
(C)200 mM NaCl
Interaction energy (kT)
Seperation distance (nm)
LW interaction energy
EDL interaction energy
AB interaction energy
Total interaction energy

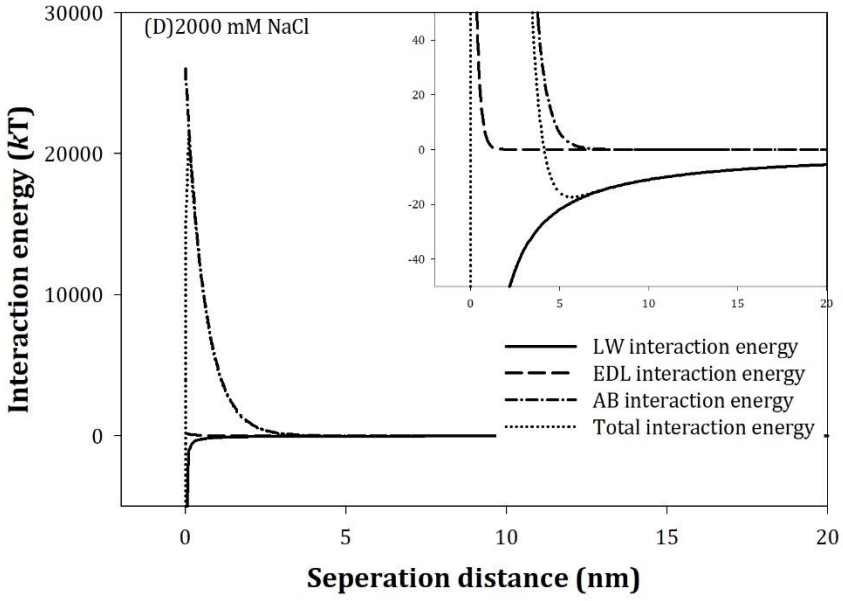

Figure 8. XDLVO interaction energy profiles for the NZVI coated with <3 k Da humic acid (A and B) and uncoated NZVI (C and D) when suspended in 200 mM and 2000 mM NaCl solutions. Unit: *k*T, where *k* is Boltzmann constant and T is absolute temperature in Kelvin.

Inspection of the interaction energy profiles also showed the presence of secondary energy minimum (Figure 8 and 9). This was due to the rapid decay rate of the AB interactions. It was previously reported that such secondary energy minimum was often responsible for the immobilization of various types of colloidal and nano particles within porous media (Wang, Xu et al. 2011, Feriancikova and Xu 2012, Johanson, Feriancikova et al. 2012, Feriancikova, Bardy et al. 2013, Johanson, Feriancikova et al. 2014). As the energy barrier and secondary energy minimum were usually located at a separation distance of < 1 nm and ~5 nm, respectively, the secondary energy minimum should be responsible for the aggregation of the coated and uncoated NZVI. This driving force for the NZVI aggregation may represent an advantage in their potential field application as the aggregation could be reversed due to various factors such as sonication and change in water chemistry.

Table 3. Depth of secondary energy minimum for the various types of NZVI when suspended in 200 mM or 2000 mM NaCl solutions (unit: *k*T), where *k* is Boltzmann constant and T is absolute temperature in Kelvin.

	NoHA	>100kDaHA	10-100kDaHA	3-10kDaHA	<3kDaHA
2000 mM	-17.3	-17.1	-15.4	-19.7	-19.4
200 mM	-15.1	-11.9	-5.2	-6.5	-7.2

It was observed that higher magnitude of the secondary energy minimum (more negative values, and more favorable for aggregation) was correlated with faster aggregation kinetics. For instance, when suspended in 200 mM NaCl solution, the aggregation kinetics of uncoated NZVI was significantly higher than the aggregation kinetics of the NZVI coated with <3 k Da humic acid (Figure 4). The depth of the secondary energy minimum was -15.1 *k*T (uncoated NZVI) and -7.2 *k*T (NZVI coated with <3k Da humic acid), respectively (Figure 8 and Table 3). The deeper secondary energy minimum was more favorable for NZVI aggregation. Indeed, as NZVI coated with <3k Da, 3-10k Da and 10-100k Da humic acid fractions all exhibited strong stability (and slower aggregation kinetics) when suspended in 200 mM NaCl solution, the depth of the secondary energy minimum was all lower than that of the uncoated NZVI (Table 3).

When suspended in $CaCl_2$ solutions, the effects of humic acid coating were less significant compared to the case of NaCl solutions (Figures 4 and 5). The difference in the depth of secondary energy was also less significant. For instance, when suspended in 4 mM $CaCl_2$, the secondary energy minimum for the uncoated NZVI and NZVI coated with <3k Da humic acid was -2.1 and -1.9 *k*T, respectively (Figure 9). The smaller magnitude in the secondary energy minimum when NZVI was suspended in $CaCl_2$ solutions compared with NaCl solutions indicated that it would be easier to reverse NZVI aggregation through chemical and physical disturbance when they were suspended in $CaCl_2$ solutions.

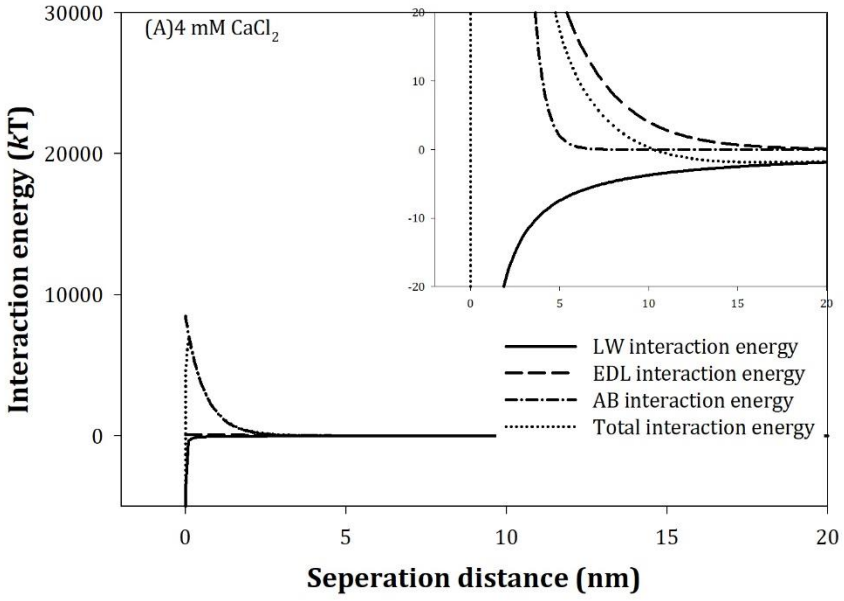
(A)4 mM CaCl2
Interaction energy (kT)
Seperation distance (nm)
LW interaction energy
EDL interaction energy
AB interaction energy
Total interaction energy

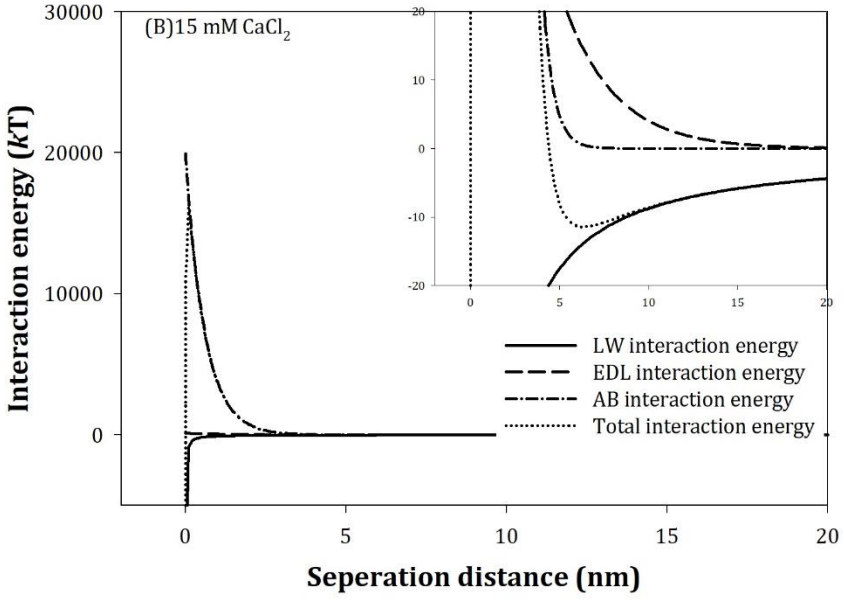
(B)15 mM CaCl2
Interaction energy (kT)
Seperation distance (nm)
LW interaction energy
EDL interaction energy
AB interaction energy
Total interaction energy

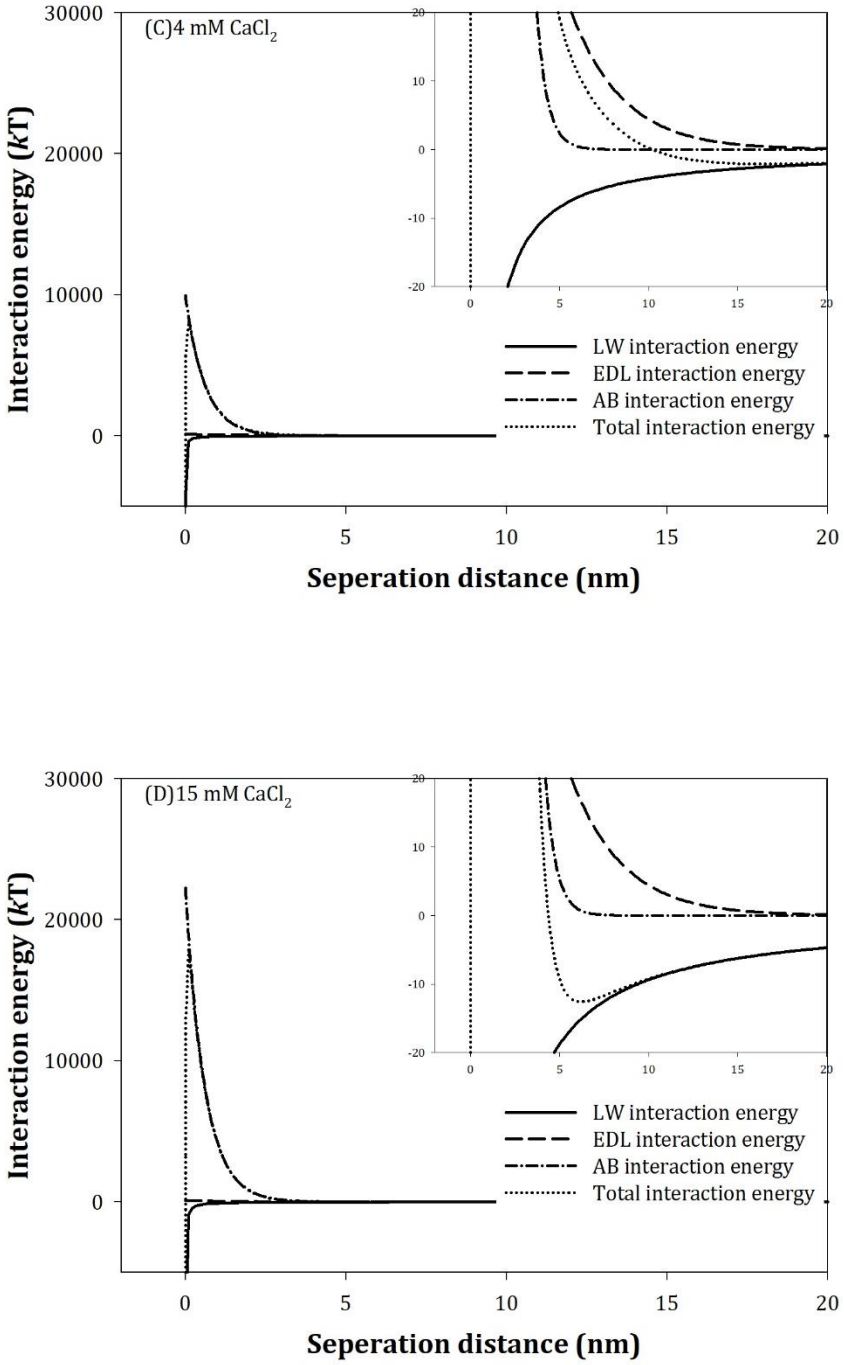

Figure 9. XDLVO interaction energy profiles for the NZVI coated with <3 k Da humic acid (A and B) and uncoated NZVI (C and D) when suspended in 4 mM and 15 mM $CaCl_2$ solutions.

The increase in ionic strength could facilitate the aggregation of uncoated and coated NZVI (Figures 4 and 5). The results presented in Figures 8 and 9, as well as Table 3 all showed that the magnitude of the secondary energy minimum increased with ionic strength, a condition that is more favorable to aggregation.

Under high ionic strength conditions (e.g., 2000 mM NaCl), the effects of humic acid coating on the aggregation kinetics of the NZVI was less significant (Figures 4 and 5). This was consistent to the observation that the depth of the secondary energy minimum was comparable under such conditions (Table 3).

4. Conclusions

The major findings from this research include:

1) Different size fractions of humic acid exhibited various effects on the stability of NZVI. In general, the smaller size fractions of humic acid could more significantly enhance the stability of NZVI under the presence of moderate to high concentrations of NaCl and moderate concentrations of $CaCl_2$.
2) The stability of both coated and uncoated NZVI decreased with increasing ionic strength.
3) The application of XDLVO theory showed that the aggregation of the coated and uncoated NZVI was primarily caused by the presence of secondary energy minimum, suggesting that the NZVI aggregation could potentially be reversed using disruption techniques such as sonication and decrease in ionic strength.
4) It was observed that there was a good correlation between the NZVI stability behavior and the depth of the secondary energy minimum.

Future work on this research could be beneficial in helping us understand more in depth the chemical causes behind the smaller humic acid fractionations increasing the stability of the NZVI. Understanding the effects pH has on the stability of the NZVI could be useful. It would also be beneficial to conduct experiments to determine the effects humic acid has on the reactivity of NZVI with targeted contaminants.

REFERENCES

Chekli, L., G. Brunetti, E. R. Marzouk, A. Maoz-Shen, E. Smith, R. Naidu, H. K. Shon, E. Lombi and E. Donner (2016). "Evaluating the mobility of polymer-stabilised zero-valent iron nanoparticles and their potential to co-transport contaminants in intact soil cores." Environmental Pollution **216**: 636-645.

Chen, K. L. and M. Elimelech (2006). "Aggregation and deposition kinetics of fullerene (C-60) nanoparticles." Langmuir **22**(26): 10994-11001.

Chen, K. L., S. E. Mylon and M. Elimelech (2006). "Aggregation kinetics of alginate-coated hematite nanoparticles in monovalent and divalent electrolytes." Environmental Science & Technology **40**(5): 1516-1523.

Crane, R. A. and T. B. Scott (2012). "Nanoscale zero-valent iron: Future prospects for an emerging water treatment technology." Journal of Hazardous Materials **211**: 112-125.

Dong, H. R., Y. K. Xie, G. M. Zeng, L. Tang, J. Liang, Q. He, F. Zhao, Y. L. Zeng and Y. A. Wu (2016). "The dual effects of carboxymethyl cellulose on the colloidal stability and toxicity of nanoscale zero-valent iron." Chemosphere **144**: 1682-1689.

Dong, H. R., F. Zhao, Q. He, Y. K. Xie, Y. L. Zeng, L. H. Zhang, L. Tang and G. M. Zeng (2017). "Physicochemical transformation of carboxymethyl cellulose-coated zero-valent iron nanoparticles (nZVI) in simulated groundwater under anaerobic conditions." Separation and Purification Technology **175**: 376-383.

Dong, H. R., F. Zhao, G. M. Zeng, L. Tang, C. Z. Fan, L. H. Zhang, Y. L. Zeng, Q. He, Y. K. Xie and Y. A. Wu (2016). "Aging study on carboxymethyl cellulose-coated zero-valent iron nanoparticles in water: Chemical transformation and structural evolution." Journal of Hazardous Materials **312**: 234-242.

Dong, W., J. Wan, T. K. Tokunaga, B. Gilbert and K. H. Williams (2017). "Transport and humification of dissolved organic matter within a semi-arid floodplain." Journal of Environmental Sciences **57**: 24-32.

Dziedzic, J., D. Wodka, P. Nowak, P. Warszyński, C. Simon and I. Kumakiri (2010). "Photocatalytic degradation of the humic species as a method of their removal from water - comparison of UV and artificial sunlight irradiation." Fizykochemiczne Problemy Mineralurgii - Physicochemical Problems of Mineral Processing **45**: 15-28.

Elimelech, M., J. Gregory, X. Jia and R. A. Williams (1998). Particle deposition and aggregation measurement, modelling, and simulation. Oxford England, Butterworth-Heinemann.

Esfahani, A. R., A. F. Firouzi, G. Sayyad and A. R. Kiasat (2014). "Transport and retention of polymer-stabilized zero-valent iron nanoparticles in saturated porous media: Effects of initial particle concentration and ionic strength." Journal of Industrial and Engineering Chemistry **20**(5): 2671-2679.

Feriancikova, L., S. L. Bardy, L. X. Wang, J. Li and S. P. Xu (2013). "Effects of Outer Membrane Protein TolC on the Transport of Escherichia coli within Saturated Quartz Sands." Environmental Science & Technology **47**(11): 5720-5728.

Feriancikova, L. and S. P. Xu (2012). "Deposition and remobilization of graphene oxide within saturated sand packs." Journal of Hazardous Materials **235**: 194-200.

Fu, F. L., D. D. Dionysiou and H. Liu (2014). "The use of zero-valent iron for groundwater remediation and wastewater treatment: A review." Journal of Hazardous Materials **267**: 194-205.

Grieger, K. D., A. Fjordbøge, N. B. Hartmann, E. Eriksson, P. L. Bjerg and A. Baun (2010). "Environmental benefits and risks of zero-valent iron nanoparticles (nZVI) for in situ remediation: Risk mitigation or trade-off?" Journal of Contaminant Hydrology **118**(3): 165-183.

Guan, X. H., Y. K. Sun, H. J. Qin, J. X. Li, I. M. C. Lo, D. He and H. R. Dong (2015). "The limitations of applying zero-valent iron technology in contaminants sequestration and the corresponding countermeasures: The development in zero-valent iron technology in the last two decades (1994-2014)." Water Research **75**: 224-248.

Hansen, A. M., T. E. C. Kraus, B. A. Pellerin, J. A. Fleck, B. D. Downing and B. A. Bergamaschi (2016). "Optical properties of dissolved organic matter (DOM): Effects of biological and photolytic degradation." Limnology and Oceanography **61**(3): 1015-1032.

He, F., M. Zhang, T. Qian and D. Zhao (2009). "Transport of carboxymethyl cellulose stabilized iron nanoparticles in porous media: Column experiments and modeling." Journal of Colloid and Interface Science **334**(1): 96-102.

He, F. and D. Zhao (2007). "Manipulating the Size and Dispersibility of Zerovalent Iron Nanoparticles by Use of Carboxymethyl Cellulose Stabilizers." Environmental Science & Technology **41**(17): 6216-6221.

Hoag, G. E., J. B. Collins, J. L. Holcomb, J. R. Hoag, M. N. Nadagouda and R. S. Varma (2009). "Degradation of bromothymol blue by 'greener' nano-scale zero-valent iron synthesized using tea polyphenols." Journal of Materials Chemistry **19**(45): 8671-8677.

Israelachvili, J. N. (1991). Intermolecular and surface forces. London ; San Diego, Academic Press.

Johanson, J. J., L. Feriancikova, A. Banerjee, D. A. Saffarini, L. X. Wang, J. Li, T. J. Grundl and S. P. Xu (2014). "Comparison of the transport of Bacteroides fragilis and Escherichia coli within saturated sand packs." Colloids and Surfaces B-Biointerfaces **123**: 439-445.

Johanson, J. J., L. Feriancikova and S. P. Xu (2012). "Influence of Enterococcal Surface Protein (esp) on the Transport of Enterococcus faecium within Saturated Quartz Sands." Environmental Science & Technology **46**(3): 1511-1518.

Kanel, S. R., R. R. Goswami, T. P. Clement, M. O. Barnett and D. Zhao (2008). "Two Dimensional Transport Characteristics of Surface Stabilized Zero-valent Iron Nanoparticles in Porous Media." Environmental Science & Technology **42**(3): 896-900.

Kheshtzar, R., A. Berenjian, N. Ganji, S.-M. Taghizadeh, M. Maleki, S. Taghizadeh, Y. Ghasemi and A. Ebrahiminezhad (2019). "Response surface methodology and reaction optimization to product zero-valent iron nanoparticles for organic pollutant remediation." Biocatalysis and Agricultural Biotechnology **21**: 101329.

Lefevre, E., N. Bossa, M. R. Wiesner and C. K. Gunsch (2016). "A review of the environmental implications of in situ remediation by nanoscale zero valent iron (nZVI): Behavior, transport and impacts on microbial communities." Science of the Total Environment **565**: 889-901.

Li, J., S. Rajasekar, C. Rajajayavel and S. Ghoshal (2016). "Transport of carboxymethyl cellulose-coated zerovalent iron nanoparticles in a sand tank: Effects of sand grain size, nanoparticle concentration and injection velocity." Chemosphere **150**: 8-16.

Li, J., Wang, X., Zhao, G., Chen, C., Chai, Z., Alsaedi, A., ... & Wang, X. (2018). Metal–organic framework-based materials: superior adsorbents for the capture of toxic and radioactive metal ions. Chemical Society Reviews, 47(7), 2322-2356.

Lin, H. and L. Guo (2020). "Variations in Colloidal DOM Composition with Molecular Weight within Individual Water Samples as Characterized by Flow Field-Flow Fractionation and EEM-PARAFAC Analysis." Environmental Science & Technology **54**(3): 1657-1667.

Mystrioti, C., N. Papassiopi, A. Xenidis, D. Dermatas and M. Chrysochoou (2015). "Column study for the evaluation of the transport properties of polyphenol-coated nanoiron." Journal of Hazardous Materials **281**: 64-69.

O'Carroll, D., B. Sleep, M. Krol, H. Boparai and C. Kocur (2013). "Nanoscale zero valent iron and bimetallic particles for contaminated site remediation." Advances in Water Resources **51**: 104-122.

Ohno, T. (2002). "Fluorescence Inner-Filtering Correction for Determining the Humification Index of Dissolved Organic Matter." Environmental Science & Technology **36**(4): 742-746.

Phenrat, T., N. Saleh, K. Sirk, R. D. Tilton and G. V. Lowry (2007). "Aggregation and Sedimentation of Aqueous Nanoscale Zerovalent Iron Dispersions." Environmental Science & Technology **41**(1): 284-290.

Raychoudhury, T., N. Tufenkji and S. Ghoshal (2012). "Aggregation and deposition kinetics of carboxymethyl cellulose-modified zero-valent iron nanoparticles in porous media." Water Research **46**(6): 1735-1744.

Saleh, N., K. Sirk, Y. Liu, T. Phenrat, B. Dufour, K. Matyjaszewski, R. D. Tilton and G. V. Lowry (2006). "Surface Modifications Enhance Nanoiron Transport and NAPL Targeting in Saturated Porous Media." Environmental Engineering Science **24**(1): 45-57.

Stefaniuk, M., P. Oleszczuk and Y. S. Ok (2016). "Review on nano zerovalent iron (nZVI): From synthesis to environmental applications." Chemical Engineering Journal **287**: 618-632.

Stubbins, A., J. F. Lapierre, M. Berggren, Y. T. Prairie, T. Dittmar and P. A. del Giorgio (2014). "What's in an EEM? Molecular Signatures Associated with Dissolved Organic Fluorescence in Boreal Canada." Environmental Science & Technology **48**(18): 10598-10606.

Su, C. M., R. W. Puls, T. A. Krug, M. T. Watling, S. K. O'Hara, J. W. Quinn and N. E. Ruiz (2013). "Travel distance and transformation of injected emulsified zerovalent iron nanoparticles in the subsurface during two and half years." Water Research **47**(12): 4095-4106.

van Oss, C. J. (2007). "Development and applications of the interfacial tension between water and organic or biological surfaces." Colloids and Surfaces B: Biointerfaces **54**(1): 2-9.

van Oss, C. J. (2008). The Extended DLVO Theory. Interface Science and Technology. C. J. van Oss, Elsevier. **16:** 31-48.

van Oss, C. J., A. Docoslis, W. Wu and R. F. Giese (1999). "Influence of macroscopic and microscopic interactions on kinetic rate constants - I. Role of the extended DLVO theory in determining the kinetic adsorption constant of proteins in aqueous media, using von Smoluchowski's approach." Colloids and Surfaces B-Biointerfaces **14**(1-4): 99-104.

van Oss, C. J. and R. F. Giese (2003). "Surface modification of clays and related materials." Journal of Dispersion Science and Technology **24**(3-4): 363-376.

van Oss, C. J., R. F. Giese and P. M. Costanzo (1990). "DLVO and Non-DLVO Interactions in Hectorite." Clays and Clay Minerals **38**(2): 151-159.

Wang, L. X., S. P. Xu and J. Li (2011). "Effects of Phosphate on the Transport of Escherichia coli O157:H7 in Saturated Quartz Sand." Environmental Science & Technology **45**(22): 9566-9573.

Weishaar, J. L., G. R. Aiken, B. A. Bergamaschi, M. S. Fram, R. Fujii and K. Mopper (2003). "Evaluation of specific ultraviolet absorbance as an indicator of the chemical composition and reactivity of dissolved organic carbon." Environmental Science & Technology **37**(20): 4702-4708.

Wu, W. J. and G. H. Nancollas (1999). "Application of the extended DLVO theory - the stability of alatrofloxacin mesylate solutions." Colloids and Surfaces B-Biointerfaces **14**(1-4): 57-66.

Xu, H. and L. Guo (2017). "Molecular size-dependent abundance and composition of dissolved organic matter in river, lake and sea waters." Water Research **117**: 115-126.

Zhao, X., W. Liu, Z. Q. Cai, B. Han, T. W. Qian and D. Y. Zhao (2016). "An overview of preparation and applications of stabilized zero-valent iron nanoparticles for soil and groundwater remediation." Water Research **100**: 245-266.

Zhou, L., T. L. Thanh, J. Gong, J. H. Kim, E. J. Kim and Y. S. Chang (2014). "Carboxymethyl cellulose coating decreases toxicity and oxidizing capacity of nanoscale zerovalent iron." Chemosphere **104**: 155-161.